Fuel 357 (2024) 129784

Contents lists available at ScienceDirect

Fuel

journal homepage: www.elsevier.com/locate/fuel

Full Length Article

Density functional theory investigation of the role of Fe doped in boron carbide nanotube as an electro-catalyst for oxygen reduction reaction in fuel cells

Ali A. Rajhi [a], Hasan Sh. Majdi [b], Chou-Yi Hsu [c,*], Anjan Kumar [d], Anmar Ghanim Taki [e], Alaauldeen A. Duhduh [f], Sagr Alamri [a], Israa Abdul Kadhim Jassem [g], Mustafa M. Kadhim [h,*]

[a] Department of Mechanical Engineering, College of Engineering, King Khalid University, Abha 61421, Saudi Arabia
[b] Department of Chemical Engineering and Petroleum Industries, Al-Mustaqbal University, 51001 Hilla, Iraq
[c] Department of Pharmacy, Chia Nan University of Pharmacy and Science, Tainan City 71710, Taiwan
[d] Department of Electronics and Communication Engineering, GLA University, Mathura 281406, India
[e] Department of Radiology & Sonar Techniques, Al-Noor University College, Nineveh, Iraq
[f] Department of Mechanical Engineering Technology, CAIT, Jazan University, Prince Mohammed Street, P.O. Box 114, Jazan 45142, Saudi Arabia
[g] College of Pharmacy, National University of Science and Technology, Dhi Qar, Iraq
[h] Medical Laboratory Techniques Department, Al-Farahidi University, Baghdad 10022, Iraq

ARTICLE INFO

Keywords:
Density functional theory
Oxygen reduction reaction
Fuel cell
Boron carbide nanotube

ABSTRACT

A critical issue in enhancing the performance of polymer electrolyte membrane fuel cells (FCs) is the slow kinetics of the cathodic oxygen reduction reaction (ORR). The development of electrocatalysts with selectivity toward the four-electron (4e) pathway and high electrochemical activity to ORR reaction is important for fuel cell applications. Within the present study, it was found that boron carbide nanotube (BC_3NT) is an encouraging ORR-EC based on density functional theory computations. In the pristine BC_3NT, the neighboring B atoms with positive charges on the surface of the material surface were incapable of providing active sites for the dissociation of O. However, the ORR catalytic activity of BC_3NT improved under the ligand effect due to the replacement of Fe atom, where there was a slight over-potential that was similar or lower than that of platinum (1 1 1), which demonstrated its superior ORR activity. The results suggest that BC-based materials are considered promising for ORR catalysis and for designing highly efficient ORR-ECs as alternatives to platinum-based catalysts.

1. Introduction

Recently, research on proton exchange membrane fuel cells (PEMFCs) with high efficiency and sustainability has become the focus of many research groups. This is due to the unique advantages of PEMFCs, such as fast starting speed, high power density, and low operating temperature. However, the sluggish kinetics of the oxygen reduction reaction (ORR) at the cathodes is a key limitation of fuel cells [1,2]. So, developing an electrocatalyst with high performance is of paramount importance for speeding up the ORR reaction at the cathodes. In spite of many research studies, the high catalytic performance and durability of fuel cells are very dependent upon precious metals, particularly platinum [3,4]. Nonetheless, the application of precious metal-based electrocatalysts is limited due to their high cost and limited availability in nature. Therefore, developing cost-effective and efficient ORR-ECs for PEMFCs is of utmost importance and urgency [5–9].

Thus far, owing to their abundant active sites and high surface-to-volume ratio, one-dimensional (1D) materials have been regarded as promising in the field of electrocatalysis [10–13]. Amongst low-dimensional materials,1D boron carbide has unique properties such as is one high quantum confinement and magnetization, large surface area, and high carrier mobility [14–16]. Moreover, many theoretical and experimental studies have been done on mixed carbon-boron nanotubes such as BC_3 [17,18]. Quantum chemical calculations have shown that the formation energy of BC3 nanotubes (BC_3NTs) is lower compared to that of carbon nanotubes since BC3 sheets can be more easily rolled into tubes. Additionally, BC_3NTs consist of only C–C and B–C bonds, which provide greater stability compared to B–B bonds, resulting in a different

* Corresponding authors.
E-mail addresses: t545316@gmail.com (C.-Y. Hsu), mkadhimmustafa@gmail.com (M.M. Kadhim).

https://doi.org/10.1016/j.fuel.2023.129784
Received 23 April 2023; Received in revised form 24 August 2023; Accepted 9 September 2023
Available online 18 September 2023

energy gap compared to carbon analogs [19]. In addition, many theoretical and experimental research studies [20–22] into improving their adsorption properties to detect the molecules of different gasses like H_2 [23] NO_2 [24–27], NO [28] and H_2S [24].

Additionally, the development of non-precious metal-based catalysts (NPMCs) can lead to more cost-effective and efficient PEMFCs and MABs as sustainable renewable energy sources [29–33]. Furthermore, pyrolyzed Fe–N–C can serve as an excellent low-cost and high-performance electrocatalyst for the ORR in PEMFCs [34–39]. The catalytic activity towards ORR and durability can be improved thanks to the existence of FeN_4 active sites in the graphitic pores or edges (FeN_4-edges) [40–43]. The formation of FeN_4-edges complexes is the cause of the enhancement in the ORR activity, capable of boosting ORR via dissociative and associative reduction mechanisms [44]. Furthermore, several studies report the interactions of heteroatoms (B/N/S/P) in the pyrolyzed Fe–N–C catalysts [45–47]. The ORR activity of these catalysts was found to be greatly affected by the presence of adjacent active sites. In particular, B and N doping in pyrolyzed Fe–N–C increased the density of adjacent FeN_4 and BN sites, which simplified O_2 dissociation and enhanced the electrocatalysis performance [48,49]. This configuration of active sites led to the side-on adhesion of O_2 and an elongation in the O–O bond for disassociating O_2 with a lower energy barrier, which made both associative as well as dissociative reduction mechanisms accessible [50]. It has been demonstrated in several studies that B-doped pyrolyzed Fe–N–C catalysts exhibit improved ORR performance [51–56]. Further studies need to be carried out regarding the dopant additions and spatial

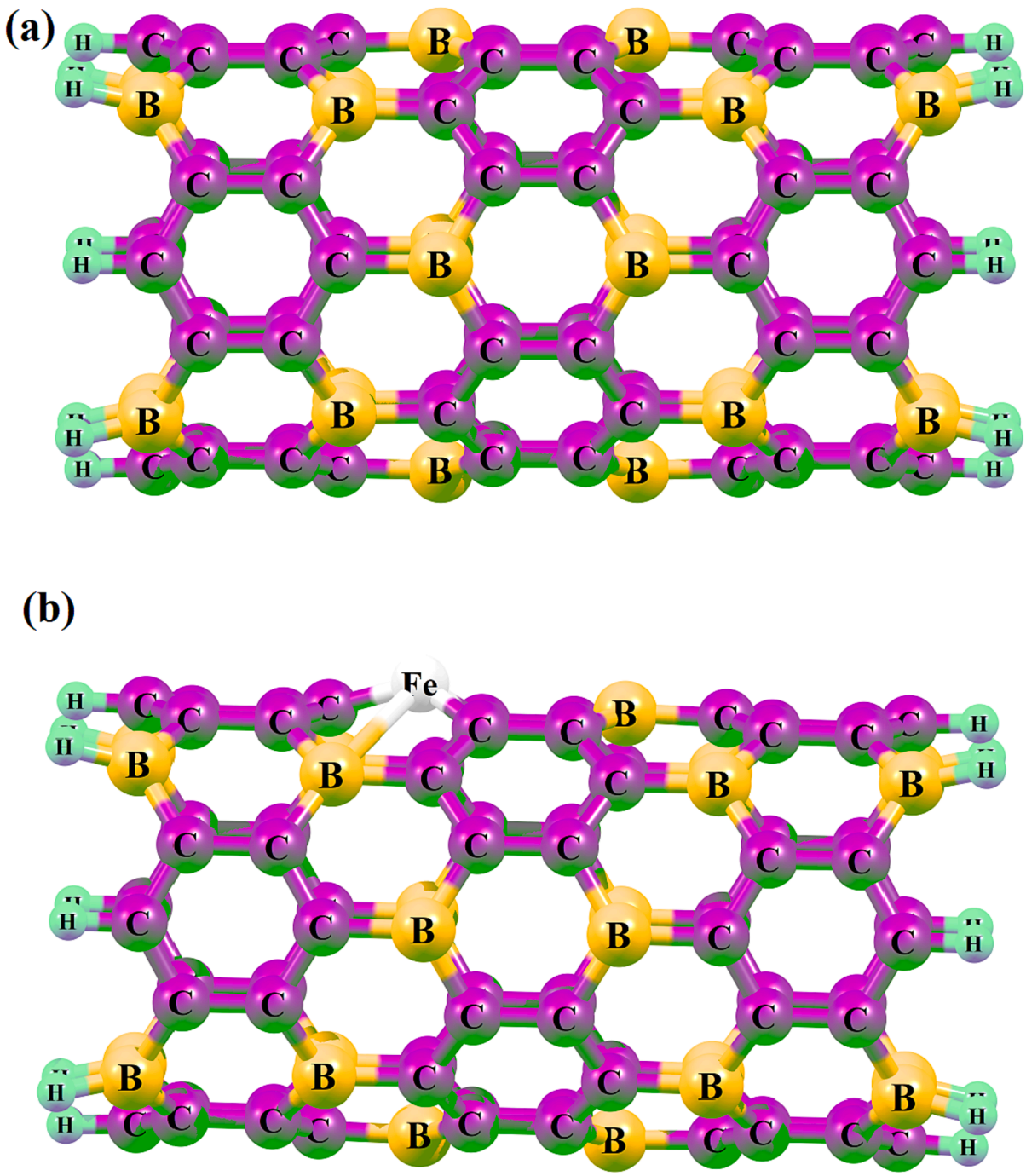

Fig. 1. The optimized structure of (a) pristine and (b) Fe-doped BC_3NT.

formation of active sites with regard to the possibility of improving the performance of Fe–N–C catalysts. In addition to experimental information, theoretical calculations such as density functional theory (DFT) can greatly enhance our understanding of various questions, including those related to the electronic structure of complex systems [57]. One example of this is Nørskov's work on metallic ORR catalysts, which have been thoroughly studied using DFT calculations [58]. The co-doping of elemental nitrogen and non-precious transition metal (TM) atoms has been shown to render graphene a highly promising electrocatalyst for the ORR process. This is thought to be due to the synergistic coupling effects that exist between the dual dopants [59,60]. Despite the promising promise of graphene- and carbon-doped catalysts for the ORR process, the theoretical understanding of the origin of their increased activity is still limited. A thorough investigation into the mechanisms at the atomic scale will therefore provide significant insight into the design of even more effective ORR catalysts.

The main goal of this work was to study the structural and chemical properties of Fe-doped BC_3-NTs as well as their effectiveness as a catalyst for the oxygen reduction reaction. Density functional theory calculations were performed to determine the effect of Fe dopant addition on the catalytic activity and stability of Fe-B-C active sites. The results indicate that the addition of Fe led to improved performance as a catalyst for ORR compared to pristine BC_3NTs. The study also suggests that advanced materials can be developed by adding dopants and controlling the location of active sites.

2. Theoretical methodology

This study utilized DFT computations with GAMESS software [61] using the GGA-PBE functional for the exchange–correlation energies [62]. The basis set used was 6–31 + G* [56]. Grimme DFT-D3 was used for examining the van der Waals forces in all of the computations [63]. For the Fe atom, we used the basis set LANL2DZ and we used 6–31 + G* for the other metals [64,65]. We set the convergence criteria for energy, force, and displacement at 10^{-5} Ha, 0.001 Ha/Å, and 0.005 Å respectively. We utilized a single-walled zigzag (8,0) model of BC_3NT by replacing boron atoms with C atoms in the (8,0) CNTs (see Fig. 1). The length and diameter of BC3-NT (8,0) zigzag were 15 Å and 7 Å respectively. It was necessary to saturate the dangling bonds to avoid the dangling effect in BC_3NT since periodic boundary conditions (PBC) were absent in the molecular computations.

In order to estimate the reaction energy barrier, have been used the CI-NEB method [66]. The reference electrode was Nørskov et al.'s hydrogen electrode (CHE) [67], which was used for evaluating the change in the reaction-free energy (ΔG). We calculated ΔG for an ORR elementary step as follows:

$$\Delta G = \Delta E + \Delta E_{ZPE} - T\Delta S + \Delta G_U + \Delta G_{pH} \quad (1)$$

here ΔE is the difference of total energy, ΔE_{ZPE} is the zero0point energy and ΔS signifies the entropy change prior to and following the reaction step. T signifies the temperature (298.15 K). DFT computations can be undertaken to directly calculate the vibration frequency and total energy of all intermediates. In general, the vibration frequency of the substrate was slight. ΔE_{ZPE} had to be computed [68]. ΔG_U = -neU, U signifies the applied electrode potential associated with the standard hydrogen electrode, and the number of the electrons was signified by n. ΔG_{pH} = -k_BTln10. pH (pH = 0 in an acid environment), ΔG_{pH} signifies Gibbs free energy correction which depends upon the concentrations of H^+ ions. Furthermore, for every elementary step that involves the proton-electron pair, the free energy G ($H^+ + e^-$) was approximated to 0.5G (H_2). Substitution energy (E_{sub}) was computed as follows for estimating and screening appropriate targets for experimental syntheses:

$$E_{sub} = E_{TM@BC_3NT} + \mu_C + \mu_B - (E_{BC_3NT} + \mu_{TM}) \quad (2)$$

where $E_{TM@BC3NT}$ signifies the total energy of Fe-embedded BC_3NT and E_{BC3NT} signifies that of perfect BC_3NT. μ_B and μ_C, respectively, signify the B atom's chemical potential in the α-rhombohedral B crystal and that of the C atom graphite lattice the chemical potential related to a single transition metal atom was signified by $\mu_{TM,}$ which was computed using their related stable bulk phases.

3. Results and discussions

3.1. Structures and electronic attributes of pristine and TM-doped BC_3NTs

By substituting elements like B, we can adjust the performance of CNTs and widen their scope of application. A BC_3 nanosheet can be rolled into a BC_3NT along the chiral vector, similar to that of a CNT. The (8,0) BC3NT is characterized by 2 hexagonal rings: the C6 ring containing 6C atoms and the C_4B_2 ring with 4C atoms and 2B atoms. Moreover, it possesses 2 types of B–C bonds with diameters of 1.59 Å and 1.58 Å, which are parallel and diagonal to the nanotube axis, respectively. There is also the presence of C–C bonds with two different lengths of approximately 1.44 Å for the pure BC_3NT as per previous theoretical research. According to the Hirshfeld analysis, the B atoms had a positive charge of 0.15e, but the C atoms had a negative charge of 0.06e, reflecting an unequal distribution of charge density on the BC_3NT compared to the (8,0) CNT counterpart.

TM can be substituted with B or C atom in the BC_3NT for buildingTM@BC_3NTs. For this purpose, we investigated two adhesion sites for TM substitution. Following the full geometry optimization, site B was found to be more favorable site than C site. The E_{sub} values of B and C sites were − 3.26 eV and + 0.73 eV, respectively, and they were more negative than those on-site B. The was a dramatic loss of electron density near the Fe in the EDD plot (see Fig. 2), which indicated the polarization of these atoms by the π electron density onto adjacent C atoms. Similar results were obtained using the Hirshfeld analysis and the atomic charge onto the Fe atom was 0.94 |e|.

3.2. The assessment of ORR catalytic activity onto the pristine and TM-doped BC_3NTs

The stability and good conductivity of the three pristine and Fe-doped BC_3NT encouraged us to investigate the possibility of using them as ORR-ECs. It goes without saying that ORR reactions at the cathodes always start with the adsorption of oxygen, which is pivotal for the entire ORR circulation and might even specify the overall reaction paths. First, Bader charge analysis was carried out and based on the results, the B, and Fe atoms have positive charges in pristine and Fe-doped BC_3NT, respectively. The positive charge populations onto the B atoms, where there was an electron transport from the B to Fe atoms, was further confirmed by the charge depletion around the B atoms. Here, the Fe atoms with a positive charge were predicted to be favorable for the adhesion of electron-donating O_2 molecules, which were capable of serving as the active site for the ORR catalysis, especially, the Fe atoms were capable of providing vacant p orbitals for activating O_2 and promoting subsequent electro-chemical steps.

Next, we investigated the various ways in which the O2 molecules can attach to the Fe-doped BC3-NT surface to determine which sites are the most significant for the oxygen reduction reaction. We identified the two adhesion complexes with the lowest energy as the most likely to become active sites during the ORR. We uniformly placed the O_2 molecules horizontally onto the surface of the nanotube and observed the interaction between them and the Fe atoms in a side-on complex (as shown in Fig. 3). Moreover, the results showed that the shortest Fe-O bond length (l) could be reduced for these two complexes as follows: complex A (2.31 Å) > complex B (2.28 Å), which agreed well with the decreasing adhesion energy of oxygen ΔE_{O2} (complex A) (-0.47 eV) > ΔE_{O2} (complex A) (-0.52 eV). However, the adsorption energies for oxygen in pristine BC_3NT are positive. In fact, the shorter Fe-O bond

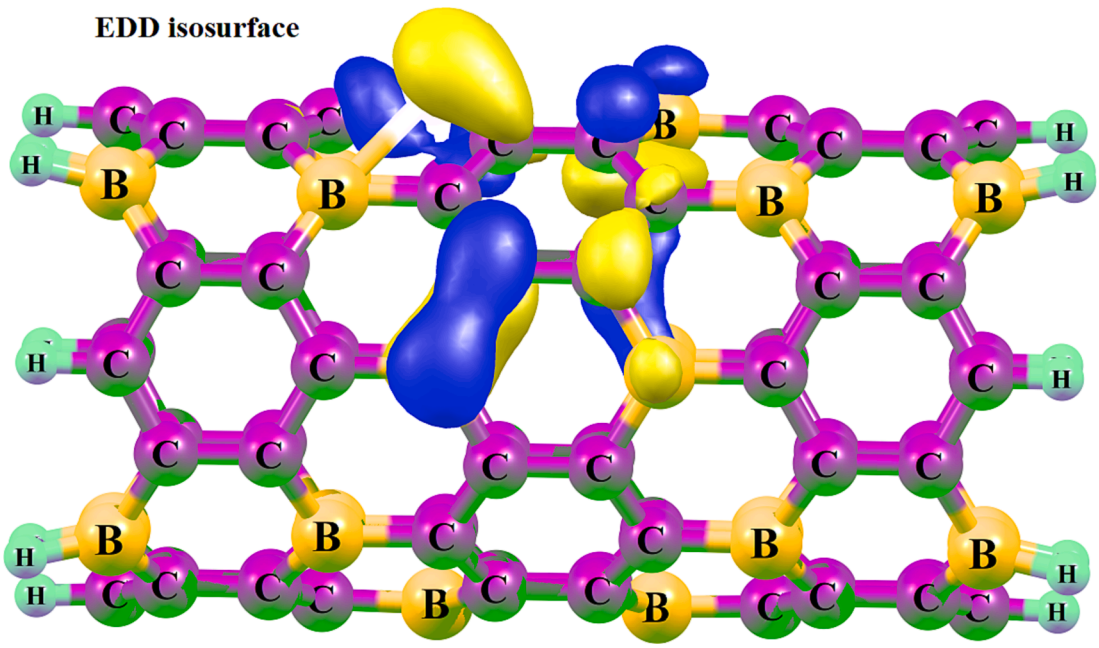

Fig. 2. The EDD isosurface (middle, isovalue = 0.04 au) of Fe@BC_3NT, the blue and yellow regions in the EDD maps correspond to the gained and loss electron density are, respectively.

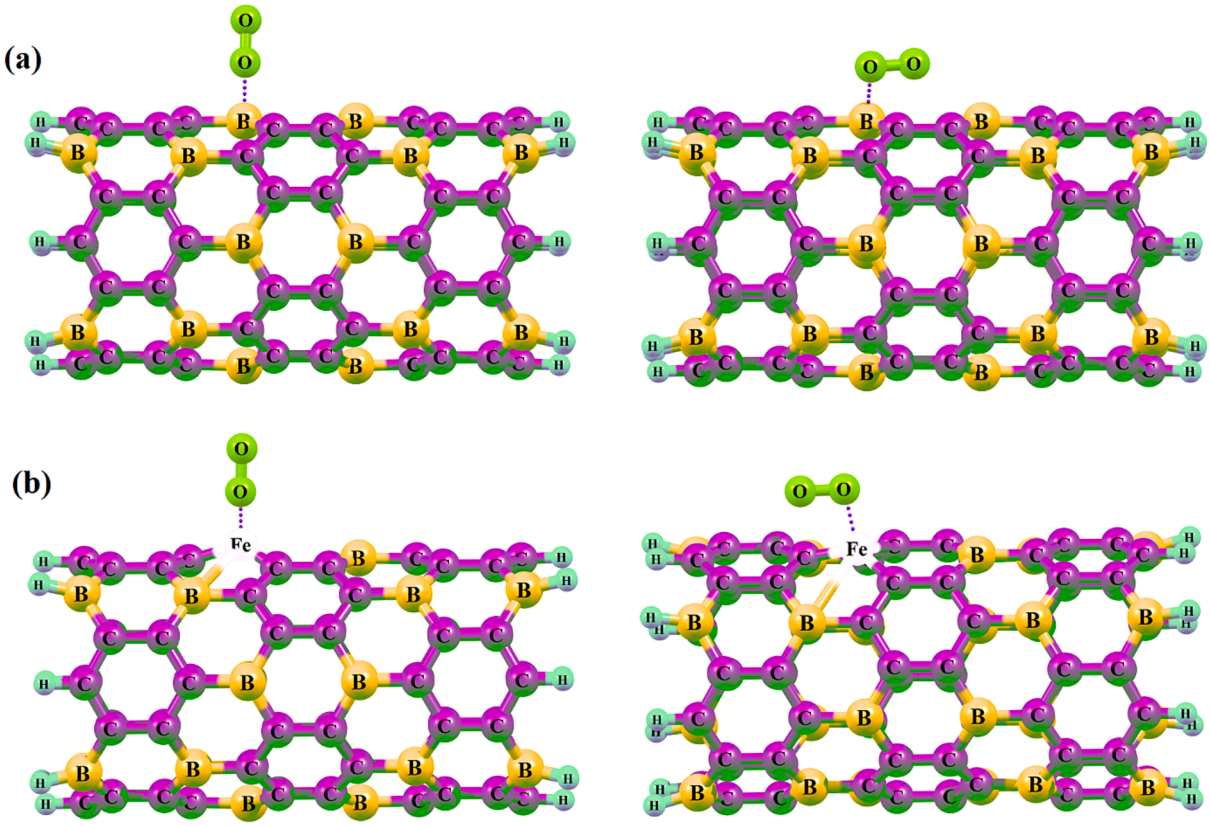

Fig. 3. Optimized geometry of a single O_2 molecule adsorbed onto pristine BC_3NT (top) and Fe@BC_3NT (bottom).

length was capable of providing greater oxygen adhesion strength onto the surface of a pristine nanotube. Among all the complexes analyzed, the adhesion energy of oxygen on the pristine BC_3NT had a positive value of 0.13 eV. This implies that O2 adhesion onto the surface of this material may be challenging. Hence, it cannot be considered as an ORR catalyst, so Fe@BC_3NT will be investigated in the subsequent computations. There was an apparent electron transport from BC_3NT to the O_2 molecule (see Fig. 3) following the adhesion of the O_2 molecule onto the surface of Fe@BC_3NT. Based on the Bader charge analysis, electron transfer was 0.78 |e| for Fe@BC_3NT. The electrons transported led to the occupation of the anti-bonding orbitals of the adhered O_2 molecule, which extended the bond length of O-O (d) dramatically from

1.23 Å to 1.35 Å for Fe@BC_3NT, which shows the possibility of effectively activating and disassociating O_2 molecules on theFe@BC_3NT surface. This demonstrated that Fe doping weakens the oxygen adhesion strength, is good for reducing protonation and improving the ORR activity.

All the intermediate complexes of ORR reaction on Fe@BC_3NT and the related Gibbs free energy plots via two paths were demonstrated in Fig. 4a for determining the most favorable 4e path on Fe@BC_3NT. As can be seen, when U is 0 V, all of the electrocatalytic steps had a downward trend. Moreover, the O_2 molecule adhered to Fe@BC_3NT had an obvious tendency for dissociation into O* species initially, which released more energy compared to the direct protonation into OOH*. Hence, the ORR reaction onto Fe@BC_3NT was capable of proceeding via the dissociation path (DP). Clearly, protonating O* into OH* was the rate-determining step onto the DP, which was accompanied by a free energy change of ΔG = -0.69 eV. Thus, the maximum value of U for ensuring the exothermic nature of all reaction steps was 0.69 V. The O* protonation into OH* onto Fe@BC_3NT was capable of producing a maximum change in the Gibbs free energy (0.41 eV at U = 1.10 V, which led to 0.41 V overpotential for ORR (lower than pure BC3NT see Fig. 4a), which was similar to that of graphitic materials doped with N (0.43– 0.73 eV) [69]. This shows the acceptable ORR catalytic activity of Fe@BC_3NT. Since the adhered O_2* could be protonated directly for forming OOH*, the association path (AP) of Fe@BC_3NT was investigated as well. As can be seen, because of the very high overpotential of 1.00 V, which was greater than the overpotential of the DP, the formation of OOH* could have been prevented effectively, Avoiding the OOH* intermediate onto Fe@BC_3NT made the production of the by-product H_2O_2 along the AP impossible. Also, the formation step of hydrogen peroxide (H_2O_2) along the ORR DP was significantly endothermic onto the Fe@BC_3NT, which suggested that the 4e DP could effectively suppress the 2 electron (2e) path. In addition to having an acceptable ORR catalytic activity, the Fe@BC_3NT also exhibited higher selectiveness for the 4e reduction path, which left water as the only product. Obviously, Based on the analysis and screening of Fe@BC_3NT, we can regard Fe@BC_3NT as an ideal ORR-EC with lower Rh-loading for fuel cells. As can be seen, it is apparent that the addition of Fe atoms has improved the ORR catalytic performance of BC_3NT.

4. Conclusions

The one-dimensional BC_3NT was found to be an encouraging ORR-EC based DFT calculation. The results demonstrated that BC_3NT had high mechanical, thermal, dynamic and thermodynamic stability. However, based on the dissociation energy barrier computations and free energy analyses, BC_3NT did not exhibit enough ORR catalytic activity by forming H_2O_2 as a byproduct. Nevertheless, after replacing the Fe atom, BC_3NT exhibited a high ORR catalytic activity, where the initial over-potential increased 0.41, which was similar or lower than that of Platinum (1 1 1) (0.45 V). We investigated the reasons for the high ORR after the replacement. Moreover, Fe-doped BC_3NT systems retained their high metallic conductance and selectivity. In fact, Fe-doping can be considered as an effective strategy for enhancing the ORR catalytic performance of BC_3NT. The results from this study can provide valuable insights into using boron carbide materials with low Fe-loading for achieving highly efficient ORR-ECs. The results also provide a strong urge to other research groups to create novel BC-doped materials for ORR catalysis, which can potentially serve as substitutes for Platinum-based catalysts.

CRediT authorship contribution statement

Ali A. Rajhi: Conceptualization, Methodology, Software, Writing – original draft. **Hasan Sh. Majdi:** Conceptualization, Methodology, Software, Validation, Writing – original draft. **Chou-Yi Hsu:** . **Anjan Kumar:** Formal analysis, Methodology, Software, Validation, Visualization, Writing – original draft, Writing – review & editing. **Anmar Ghanim Taki:** Methodology, Software, Writing – original draft, Validation. **Alaauldeen A. Duhduh:** Conceptualization, Investigation, Methodology, Software, Writing – original draft, Writing – review & editing. **Sagr Alamri:** . **Israa Abdul Kadhim Jassem:** Conceptualization, Methodology, Software, Validation, Writing – original draft. **Mustafa M. Kadhim:** Writing – review & editing, Methodology, Investigation, Formal analysis.

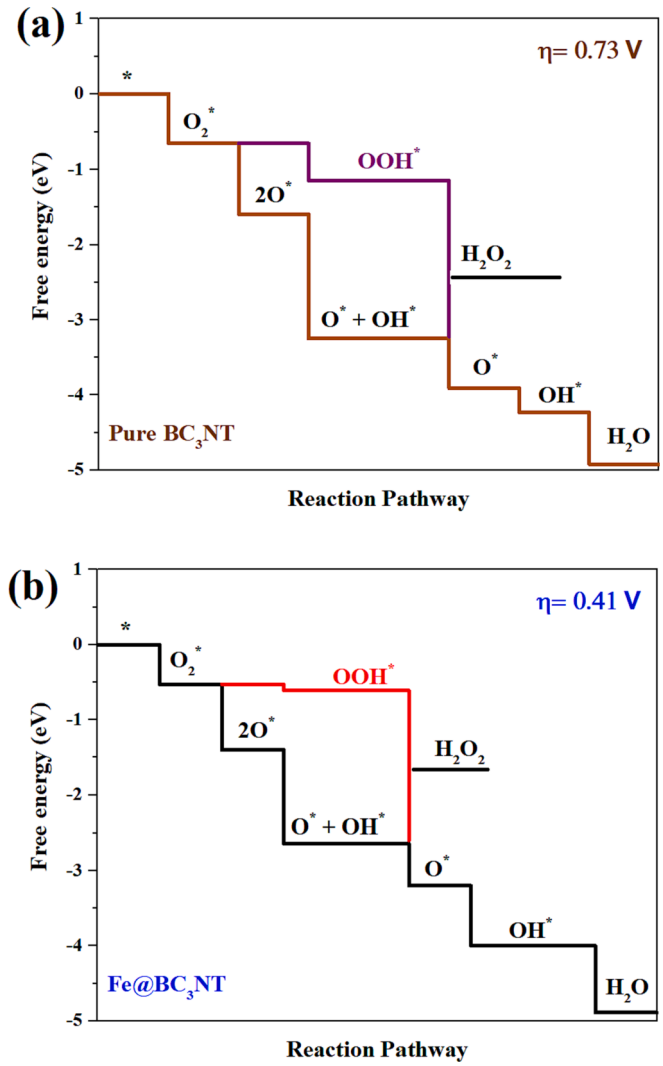

Fig. 4. The free energy diagram of ORR along dissociation and association paths for (a) pure BC_3NT and (b) Fe@BC_3NT. The black grid represents the rate-determining step (RDS) of the dissociation path.

Declaration of Competing Interest

The authors declare that they have no known competing financial interests or personal relationships that could have appeared to influence the work reported in this paper.

Data availability

No data was used for the research described in the article.

Acknowledgments

The authors extend their appreciation to the Deanship of Scientific Research at King Khalid University, Saudi Arabia for funding this work

through the Research Group Program under Grant No. RGP. 2/282/44.

References

[1] Debe MK. Electrocatalyst approaches and challenges for automotive fuel cells. Nature 2012;486:43–51.
[2] Huang Q, Jiang S, Wang Y, Jiang J, Chen Y, Xu J, et al. Highly active and durable triple conducting composite air electrode for low-temperature protonic ceramic fuel cells. Nano Res 2023:1–9.
[3] Rabis A, Rodriguez P, Schmidt TJ. Electrocatalysis for polymer electrolyte fuel cells: recent achievements and future challenges. ACS Catal 2012;2:864–90.
[4] Yu X, Ye S. Recent advances in activity and durability enhancement of Pt/C catalytic cathode in PEMFC. J Power Sources 2007;1:133–44.
[5] Stoerzinger KA, Risch M, Han B, Shao-Horn Y. Recent insights into manganese oxides in catalyzing oxygen reduction kinetics. ACS Catal 2015;5:6021–31.
[6] Cao R, Lee JS, Liu M, Cho J. Recent progress in non-precious catalysts for metal-air batteries. Adv Energy Mater 2012;2:816–29.
[7] Sun T, Wu Q, Che R, Bu Y, Jiang Y, Li Y, et al. Alloyed Co–Mo nitride as high-performance electrocatalyst for oxygen reduction in acidic medium. ACS Catal 2015;5:1857–62.
[8] Yang C, Guo R, Jing X, Li P, Yuan J, Wu Y. Degradation mechanism and modeling study on reversible solid oxide cell in dual-mode—A review. Int J Hydrogen Energy 2022;47:37895–928.
[9] Yu D, Duan C, Gu B. Design and evaluation of a novel plan for thermochemical cycles and PEM fuel cells to produce hydrogen and power: Application of environmental perspective. Chemosphere 2023;334:138935.
[10] Yun Q, Lu Q, Zhang X, Tan C, Zhang H. Three-dimensional architectures constructed from transition-metal dichalcogenide nanomaterials for electrochemical energy storage and conversion. Angew Chem Int Ed 2018;57:626–46.
[11] Weng CC, Ren JT, Yuan ZY. Transition metal phosphide-based materials for efficient electrochemical hydrogen evolution: a critical review. ChemSusChem 2020;13:3357–75.
[12] Wang W, Xu X, Zhou W, Shao Z. Recent progress in metal-organic frameworks for applications in electrocatalytic and photocatalytic water splitting. Adv Sci 2017;4:1600371.
[13] Li Y, Guo S. Noble metal-based 1D and 2D electrocatalytic nanomaterials: Recent progress, challenges and perspectives. Nano Today 2019;28:100774.
[14] Ma R, Bando Y. High purity single crystalline boron carbide nanowires. Chem Phys Lett 2002;364:314–7.
[15] Guan Z, Gutu T, Yang J, Yang Y, Zinn AA, Li D, et al. Boron carbide nanowires: low temperature synthesis and structural and thermal conductivity characterization. J Mater Chem 2012;22:9853–60.
[16] Li H-M, Li G-X, Li L, Wu J-Z, Yao Z-P, Zhang T. Combustion characteristics and concentration measurement of ADN-based liquid propellant with electrical ignition method in a combustion chamber. Fuel 2023;344:128142.
[17] Belasfar K, Houmad M, Boujnah M, Benyoussef A, Kenz AE. First-principles study of BC3 monolayer as anodes for lithium-ion and sodium-ion batteries applications. J Phys Chem Solid 2020;139:109319.
[18] Song H, Gao J, Wu L. Fluorouracil drug sensing characteristics of pristine and Al-doped BC3 nanosheets: Quantum chemical study. Comput Theor Chem 2020;1182:112847.
[19] Su W, Chang C, Lin M, Li T. Electronic structures and work functions of BC 3 nanotubes: A first-principle study. J Appl Phys 2011;110:014312.
[20] Niu F, Liu J-M, Tao L-M, Wang W, Song W-G. Nitrogen and silica co-doped graphene nanosheets for NO 2 gas sensing. J Mater Chem A 2013;1:6130–3.
[21] Niu F, Tao L-M, Deng Y-C, Wang Q-H, Song W-G. Phosphorus doped graphene nanosheets for room temperature NH 3 sensing. New J Chem 2014;38:2269–72.
[22] Rahimi R, Solimannejad M. Gas-sensing performance of BC 3 nanotubes for detecting poisonous cyanogen gas: a periodic DFT approach. New J Chem 2021;45:11574–84.
[23] Zhang J, Wu J, Wu L. Sensing and monitoring of edifenphos molecules based on the quantum chemical approach. J Mol Model 2020;26:1–7.
[24] Star A, Joshi V, Skarupo S, Thomas D, Gabriel J-C-P. Gas sensor array based on metal-decorated carbon nanotubes. J Phys Chem B 2006;110:21014–20.
[25] Espinosa E, Ionescu R, Bittencourt C, Felten A, Erni R, Van Tendeloo G, et al. Metal-decorated multi-wall carbon nanotubes for low temperature gas sensing. Thin Solid Films 2007;515:8322–7.
[26] Li H-M, Li G-X, Li L. Comparative investigation on combustion characteristics of ADN-based liquid propellants in inert gas and oxidizing gas atmospheres with resistive ignition method. Fuel 2023;334:126742.
[27] Feng X, Wang B, Gao G, Gao S, Xie C, Shi J-W. MnyCo3− yOx bimetallic oxide prepared by ultrasonic technology for significantly improved catalytic performance in the reduction of NOx with NH3. Fuel 2023;352:129159.
[28] Aghaei SM, Monshi M, Torres I, Zeidi S, Calizo I. DFT study of adsorption behavior of NO, CO, NO2, and NH3 molecules on graphene-like BC3: a search for highly sensitive molecular sensor. Appl Surf Sci 2018;427:326–33.
[29] Chen K, Ci S, Xu Q, Cai P, Li M, Xiang L, et al. Iron-incorporated nitrogen-doped carbon materials as oxygen reduction electrocatalysts for zinc-air batteries. Chin J Catal 2020;41:858–67.
[30] Ma W, Wan H, Zhang L, Zheng JY, Zhou Z. Single-atom catalysts for electrochemical energy storage and conversion, Journal of Energy. Chemistry 2021;63:170–94.
[31] Sun M, Gong S, Zhang Y-X, Niu Z. A perspective on the PGM-free metal–nitrogen–carbon catalysts for PEMFC, Journal of Energy. Chemistry 2022;67:250–4.
[32] Lu C, Xu C, Sun W, Ren R, Qiao J, Wang Z, et al. Enhancing catalytic activity of CO2 electrolysis by building efficient and durable heterostructure for solid oxide electrolysis cell cathode. J Power Sources 2023;574:233134.
[33] Li L, Jia S, Cao M, Ji Y, Qiu H, Zhang D. Research progress on transition metal sulfide-based materials as cathode materials for zinc-ion batteries. J Storage Mater 2023;67:107614.
[34] Shi W, Wang Y-C, Chen C, Yang X-D, Zhou Z-Y, Sun S-G. A mesoporous Fe/N/C ORR catalyst for polymer electrolyte membrane fuel cells. Chin J Catal 2016;37:1103–8.
[35] Lv Y-R, Zhai X-J, Wang S, Xu H, Wang R, Zang S-Q. 3D-ordered macroporous N-doped carbon encapsulating Fe-N alloy derived from a single-source metal-organic framework for superior oxygen reduction reaction. Chin J Catal 2021;42:490–500.
[36] Li Y, Xu K, Zhang Q, Zheng Z, Li S, Zhao Q, et al. One-pot synthesis of FeNxC as efficient catalyst for high-performance zinc-air battery, Journal of Energy. Chemistry 2022;66:100–6.
[37] Yang Y, Lai L, Wei L, Chen Y. Degradation: A critical challenge for M-N–C electrocatalysts, Journal of Energy. Chemistry 2021;63:667–74.
[38] Dou Y, Wang A, Zhao L, Yang X, Wang Q, Sudi MS, et al. Boosted hydrogen evolution reaction for a nitrogen-rich azo-bridged metallated porphyrin network. J Colloid Interface Sci 2023;650:943–50.
[39] Huang K, Xu Q, Ying Q, Gu B, Yuan W. Wireless strain sensing using carbon nanotube composite film. Compos B Eng 2023;256:110650.
[40] Jiang R, Li L, Sheng T, Hu G, Chen Y, Wang L. Edge-site engineering of atomically dispersed Fe–N4 by selective C-N bond cleavage for enhanced oxygen reduction reaction activities. J Am Chem Soc 2018;140:11594–8.
[41] Ma R, Lin G, Ju Q, Tang W, Chen G, Chen Z, et al. Edge-sited Fe-N4 atomic species improve oxygen reduction activity via boosting O2 dissociation. Appl Catal B 2020;265:118593.
[42] Matsumoto K, Onoda A, Kitano T, Sakata T, Yasuda H, Campidelli S, et al. Thermally Controlled Construction of Fe–N x Active Sites on the Edge of a Graphene Nanoribbon for an Electrocatalytic Oxygen Reduction Reaction. ACS Appl Mater Interfaces 2021;13:15101–12.
[43] Ding X-B, Zhang L, Qin Y-H, Yang L, Wang C, Peng C. Highly porous Fe/N/C catalyst for oxygen reduction: the importance of pores. Chem Commun 2021;57:6935–8.
[44] Saputro AG, Maulana AL, Fathurrahman F, Mahyuddin MH, Agusta MK, Shukri G, et al. Formation of Tilted FeN4 Configuration as the Origin of Oxygen Reduction Reaction Activity Enhancement on a Pyrolyzed Fe-NC Catalyst with FeN4-Edge Active Sites. J Phys Chem C 2021;125:19682–96.
[45] Saputro AG, Kasai H. Oxygen reduction reaction on neighboring Fe–N 4 and quaternary-N sites of pyrolized Fe/N/C catalyst. PCCP 2015;17:3059–71.
[46] Dipojono HK, Saputro AG, Fajrial AK, Agusta MK, Akbar FT, Rusydi F, et al. Oxygen reduction reaction mechanism on a phosporus-doped pyrolyzed graphitic Fe/N/C catalyst. New J Chem 2019;43:11408–18.
[47] Wang Z, Dai L, Yao J, Guo T, Hrynsphan D, Tatsiana S, et al. Enhanced adsorption and reduction performance of nitrate by Fe–Pd–Fe3O4 embedded multi-walled carbon nanotubes. Chemosphere 2021;281:130718.
[48] Fajrial AK, Saputro AG, Agusta MK, Rusydi F, Dipojono HK. First principles study of oxygen molecule interaction with the graphitic active sites of a boron-doped pyrolyzed Fe–N–C catalyst. PCCP 2017;19:23497–504.
[49] Fajrial AK, Abdulkarim MF, Saputro AG, Agusta MK, Dipojono HK. Boron and nitrogen co-doping configuration on pyrolyzed Fe-N4/C catalyst. Procedia Eng 2017;170:131–5.
[50] Saputro AG, Fajrial AK, Maulana AL, Fathurrahman F, Agusta MK, Akbar FT, et al. Dissociative oxygen reduction reaction mechanism on the neighboring active sites of a boron-doped Pyrolyzed Fe–N–C catalyst. J Phys Chem C 2020;124:11383–91.
[51] Yuan K, Sfaelou S, Qiu M, Lützenkirchen-Hecht D, Zhuang X, Chen Y, et al. Synergetic contribution of boron and Fe–N x species in porous carbons toward efficient electrocatalysts for oxygen reduction reaction. ACS Energy Lett 2017;3:252–60.
[52] Zhao YM, Liao LM, Yu GQ, Wei PJ, Liu JG. B-Doped Fe/N/C Porous Catalyst for High-Performance Oxygen Reduction in Anion-Exchange Membrane Fuel Cells. ChemElectroChem 2019;6:1754–60.
[53] Jiao L, Xu W, Zhang Y, Wu Y, Gu W, Ge X, et al. Boron-doped Fe-NC single-atom nanozymes specifically boost peroxidase-like activity. Nano Today 2020;35:100971.
[54] Zhao X, Li X, Bi Z, Wang Y, Zhang H, Zhou X, et al. Boron modulating electronic structure of FeN4C to initiate high-efficiency oxygen reduction reaction and high-performance zinc-air battery, Journal of Energy. Chemistry 2022;66:514–24.
[55] Wang A, Dou Y, Yang X, Wang Q, Sudi MS, Zhao L, et al. Efficient oxygen evolution reaction from iron-molybdenum nitride/molybdenum oxide heterostructured composites. Dalton Trans 2023;52:11234–42.
[56] Kong L, Liu Y, Dong L, Zhang L, Qiao L, Wang W, et al. Enhanced red luminescence in CaAl 12 O 19: Mn 4+ via doping Ga 3+ for plant growth lighting. Dalton Trans 2020;49:1947–54.
[57] Kohn W. Nobel Lecture: Electronic structure of matter—wave functions and density functionals. Rev Mod Phys 1999;71:1253.
[58] Greeley J, Stephens I, Bondarenko A, Johansson TP, Hansen HA, Jaramillo T, et al. Alloys of platinum and early transition metals as oxygen reduction electrocatalysts. Nat Chem 2009;1:552–6.
[59] Lu Z, Xu G, He C, Wang T, Yang L, Yang Z, et al. Novel catalytic activity for oxygen reduction reaction on MnN4 embedded graphene: A dispersion-corrected density functional theory study. Carbon 2015;84:500–8.

[60] Liang W, Chen J, Liu Y, Chen S. Density-functional-theory calculation analysis of active sites for four-electron reduction of O2 on Fe/N-doped graphene. ACS Catal 2014;4:4170–7.
[61] Schmidt MW, Baldridge KK, Boatz JA, Elbert ST, Gordon MS, Jensen JH, et al. General atomic and molecular electronic structure system. J Comput Chem 1993; 14:1347–63.
[62] Perdew JP, Burke K, Ernzerhof M. Generalized gradient approximation made simple. Phys Rev Lett 1996;77:3865.
[63] Grimme S. Semiempirical GGA-type density functional constructed with a long-range dispersion correction. J Comput Chem 2006;27:1787–99.
[64] Deng J, Lei Y, Wen S, Chen Z. Modeling interactions between ethyl xanthate and Cu/Fe ions using DFT/B3LYP approach. Int J Miner Process 2015;140:43–9.
[65] Altimari US, Mireya Romero Parra R, Ketut Acwin N, Majdi A, Kadhim MM, Alawsi T, et al. Computational study of the effect of Fe-doping on the sensing characteristics of BC3 nano-sheet toward sulfur trioxide. Comput Theor Chem 2022:113805.
[66] Henkelman G, Uberuaga BP, Jónsson H. A climbing image nudged elastic band method for finding saddle points and minimum energy paths. J Chem Phys 2000; 113:9901–4.
[67] Rossmeisl J, Logadottir A, Nørskov JK. Electrolysis of water on (oxidized) metal surfaces. Chem Phys 2005;319:178–84.
[68] Ryde U. A fundamental view of enthalpy–entropy compensation. MedChemComm 2014;5:1324–36.
[69] Yu D, Zhang Q, Dai L. Highly efficient metal-free growth of nitrogen-doped single-walled carbon nanotubes on plasma-etched substrates for oxygen reduction. J Am Chem Soc 2010;132:15127–9.